energies

Article

Performance Evaluation of a Commercial Greenhouse in Canada Using Dehumidification Technologies and LED Lighting: A Modeling Study

Alexander Nauta, Jingjing Han, Syeda Humaira Tasnim and William David Lubitz *

School of Engineering, University of Guelph, Guelph, ON N1G 2W1, Canada
* Correspondence: wlubitz@uoguelph.ca; Tel.: +1-519-824-4120 (ext. 54387)

Abstract: In this study, a lumped parameter model, developed and extensively validated by the authors, is used to simulate the impact of three different dehumidification technologies (mechanical refrigeration dehumidifier, liquid desiccant dehumidifier, and a heat recovery ventilation unit), at a commercial greenhouse growing potted roses in southwestern Ontario, Canada. Typical meteorological year (TMY) data from nearby Vineland, Ontario was used to provide the external weather data used in the model. Each greenhouse bay containing a dehumidification unit was simulated for spring, fall, and winter conditions. The potential reductions in energy use (kWh), greenhouse gas emissions (kg CO_{2e}), and operating cost were estimated for each test case. The potential energy savings from switching from high-pressure sodium (HPS) to light-emitting diode (LED) lights were also examined. The simulation results showed that switching to LED lamps could reduce the electrical energy usage by up to 60% but would increase the space heating requirements. The expected energy-savings from using dehumidification equipment and switching from HPS to LED lighting in Canadian greenhouses is underrepresented in the literature. With the industry growing in the region, this study provides insight into the expected impact that these systems will have on the energy use in commercial greenhouses.

Keywords: greenhouse microclimate; dehumidification; mechanical refrigeration dehumidifier; liquid desiccant dehumidifier; heat recovery ventilation

Citation: Nauta, A.; Han, J.; Tasnim, S.H.; Lubitz, W.D. Performance Evaluation of a Commercial Greenhouse in Canada Using Dehumidification Technologies and LED Lighting: A Modeling Study. *Energies* **2023**, *16*, 1015. https://doi.org/10.3390/en16031015

Academic Editor: Pavel A. Strizhak

Received: 1 December 2022
Revised: 12 January 2023
Accepted: 13 January 2023
Published: 17 January 2023

1. Introduction

The province of Ontario has a large and growing greenhouse sector that accounted for 60% of the greenhouse area in Canada and generated 70% of the greenhouse farm gate value in 2017 [1]. Ontario greenhouse production is experiencing rapid growth recently due to the demand for high-quality, locally grown vegetables, flowers, and cannabis [2]. In 2018, the Ontario greenhouse sector consumed 7.5 TWh of energy, 73% in the form of natural gas and 18% as electricity [1]. The heating energy use in Ontario is highest at the beginning and end of the season; increasing the year-round production would make the energy costs an even greater share of the total costs [3]. Ontario growers must also contend with hot and humid summer conditions when solar radiation can generate excess heat in greenhouse environments [4]. The control of excess heat or humidity in conventional greenhouses is usually achieved by venting, however, dehumidification technologies can be considered to reduce the simultaneous loss of sensible heat via ventilation. Ontario greenhouses need to provide supplemental light during the late fall, winter, and early spring, when natural lighting is insufficient for many crops, most commonly using traditional high-pressure sodium (HPS) lamps or more efficient Light Emitting Diodes (LEDs).

Three different dehumidification technologies were considered in this study. The mechanical refrigeration dehumidifier (MRD) removes water vapor from the air using an electrically-driven refrigeration cycle: humid greenhouse air is passed over a surface cooled by a refrigerant that is below the dew point temperature of the air [5]. The condensation occurs that also releases latent heat into the greenhouse air, which can reduce the heating loads.

An MRD unit was found to be more effective at controlling humidity than an air-to-air heat exchanger at a Saskatchewan, Canada greenhouse, particularly when the outdoor air was very humid [6]. The MRD required less maintenance and reduced the plant losses caused by high humidity from 43.3% to 0.9% [6]. As the MRD released heat into the greenhouse from condensation and electrical waste heat, it was found that 47.8% and 30.3% of the electricity costs of running the unit in 2012 and 2013, respectively, were recovered as heat released into the greenhouse [6].

An MRD-equipped greenhouse (2320 m^2) in France was monitored during the winter conditions [7]. The analysis showed that using the MRD decreased the heating requirements and prevented the leaf temperatures from reaching the dew point [7]. It was estimated that the unit consumed 6 to 8.5 times less energy than traditional heating-venting [7]. However, the authors noted that the system economic feasibility was highly dependent on natural gas and electricity prices, and a reduction in overall energy use may not necessarily translate into financial savings.

Liquid desiccant dehumidification (LDD) removes water vapor from the air using a desiccant solution, typically calcium chloride, lithium bromide, or lithium chloride [5]. The water vapor in the air is absorbed into the solution due to the difference in the vapor pressure deficit (VPD), which results in the dilution of the desiccant material [5]. The desiccant solution is regenerated using a heat source to desorb and remove the water from the system.

Italian researchers compared two greenhouses over three years that were identical, except one had an AGAM 1020 liquid desiccant unit, and found winter energy savings of 9.6% to 15.6% in the LDD-equipped greenhouse [8]. When the inside-to-outside temperature difference decreased, the unit could supply up to 100% of the energy demand required for space heating [8].

Heat recovery ventilation (HRV) removes water vapor from the greenhouse through air exchange. The outgoing air is used to warm the incoming air through a heat exchanger, reducing the heat loss. The effectiveness of HRV is very dependent on outdoor air conditions. An HRV-equipped greenhouse in Saskatoon, Canada was effective at managing the humidity in the colder seasons but was not as effective in the summer during the early morning and night [9]. It was estimated that the use of the HRV reduced the percentage of time when the RH exceeded 75% in the summer to 25.7%, compared with 68% without the unit [9].

Researchers in Sweden evaluated the impact of an HRV in a naturally ventilated tomato greenhouse [10]. Simulation results with the HRV saw the thermal energy reduced by 15% to 17% during April to September [10]. The results suggested that additional incoming air preheating may be necessary in the cold weather to prevent a drop in the indoor temperature [10]. Some sources suggest that the HRV units may become clogged with ice when used in the cold weather (below −6 °C), which can be mitigated when the units have a defrost cycle [11]. A bylaw in Whitehorse, Yukon, Canada states that the HRV units in the city must have a sensible heat recovery of 64% when the outdoor air temperature is −25 °C [12].

Another possible energy saving technology available for northern greenhouses is switching from HPS lamps to LED lighting. While electrical energy savings typically can be accurately estimated using the lamp lighting efficacy (μmol PAR·J^{-1}), each lamp type also releases different amounts and types of heat into the greenhouse, potentially changing the amount of needed supplemental heating. Most greenhouse energy models in the literature that consider supplemental lighting [13] assume 40 to 50% of the electrical energy used by the lamp is released to the greenhouse as heat for LEDs, and 60 to 70% for HPS lamps [14]. These values include only radiative and convective heat transfer from the lamp and exclude the portion of electrical input that is converted to photosynthetically active radiation (PAR).

However, much of the PAR from a lamp that reaches the crop canopy can be assumed to eventually become heat (typically latent). Typically, less than 3% of the PAR reaching the crops is converted to biomass [15], while the rest is either reflected or absorbed by the canopy.

The estimated energy savings associated with converting from HPS to LED lighting in greenhouses was examined by Dutch researchers [16] using a validated greenhouse model (GreenLight) to estimate the heating and lighting energy requirements with either LED or HPS lamps [16]. Switching to LEDs was associated with an estimated 40% average reduction in the lighting electricity use, and an overall annual energy savings of 10% to 25% when accounting for the differences in supplemental heating requirements [16]. The GreenLight model was designed to predict the energy use of greenhouses with LED and HPS lights, and the validation suggested an error range on predicting heating requirements of 1% to 12% [16]. However, the model was only validated at a single greenhouse and the upper error range of the estimated energy usage is quite high for seasonal energy simulations [17].

In the current study, the impact of using three dehumidification units (MRD, LDD, and HRV) in the spring, fall, and winter conditions was simulated using a greenhouse energy model in the southwestern Ontario context. The seasonal energy impact of using LED lights instead of HPS lamps was also examined. The potential energy (kWh), greenhouse gas (kg CO_{2e}), and cost ($CAD) reductions were estimated for each test case. The expected energy savings that Canadian growers can expect to achieve by using dehumidification equipment and switching from HPS to LED lighting is underrepresented in the literature. This study seeks to address this lack of information using a novel greenhouse energy model that has been extensively validated against the measured data.

2. Methodology

2.1. Site Information

This study examines a potted rose greenhouse with exhaust fans on the south wall (560 W for each fan). Ceiling energy curtains were present, while supplemental lighting was provided by 600 W HPS fixtures. The supplemental heating was delivered via hot water pipes at three different heights. Evaporative cooling pads were present on the north wall but only used in the summer. CO_2 burners were extensively used during the daytime in the winter to increase CO_2 concentration (units released 0.38 kg $CO_2 \cdot min^{-1}$), but infrequently used in the other seasons. Figure 1 shows a schematic of one of the bays (which had the MRD unit installed). Table 1 lists the dimensions and other information of each of the three greenhouse bays considered in the study.

Table 1. Greenhouse properties.

	Section A	Section B	Section C
Length (m)	65.8	65.8	65.8
Width (m)	25.6	25.6	38.4
Area (m^2)	1684	1684	2527
Gutter height (m)	4.3	4.3	4.3
Roof height (m)	6.0	6.0	6.0
Volume (m^3)	8675	8675	13013
Crop covered fraction	0.8	0.8	0.8
Crop type	Potted rose	Potted rose	Potted rose
Roof material	Double layer PE	Double layer PE	Double layer PE
Number of exhaust fans	8	8	12
Number of HPS fixtures	120	120	150
Dehumidification type	MRD	LDD	HRV

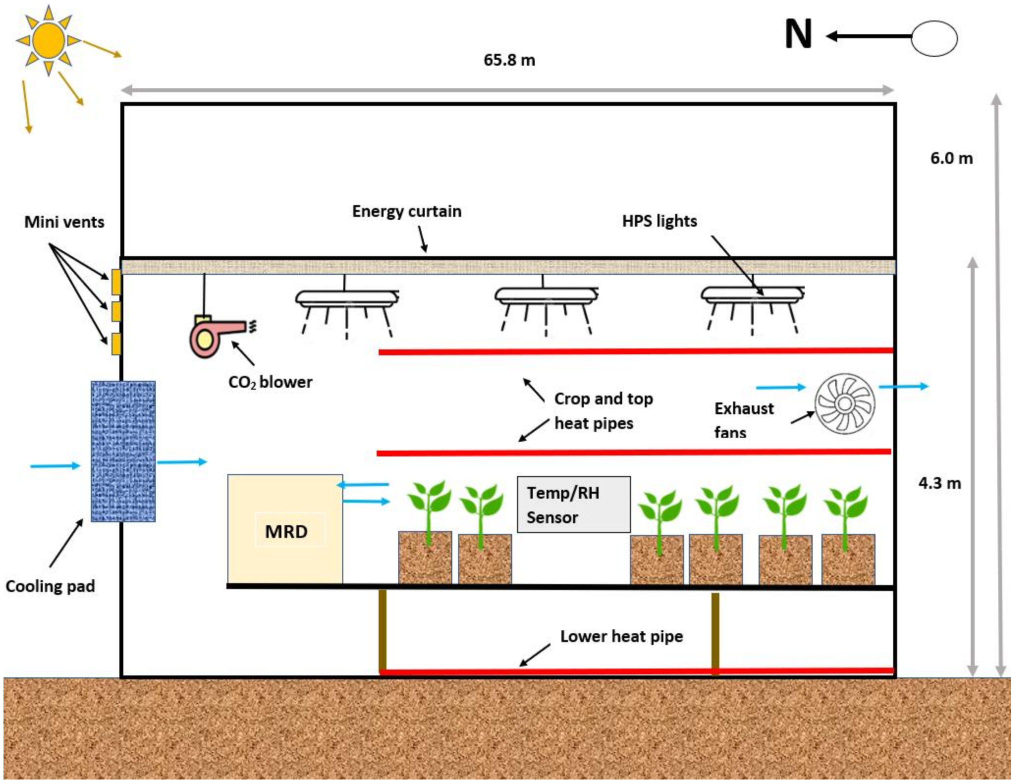

Figure 1. Cross-section schematic of Section A (with MRD).

2.2. Model Configuration

This study used a lumped parameter model developed and extensively validated by the authors and described in detail in previous work [18–20]. The model predicts the time-series temperature of various greenhouse elements, such as the indoor air and soil, based on external weather data and system controls, using a simulation time step of six seconds. It predicts the absolute humidity of the indoor air based on the crop type and greenhouse controls (ventilation, dehumidification technology, CO_2 burners). The model has been validated in each season against the experimental data from the site, with strong correlation for both the indoor air temperature and the RH [18,20]. It has also been validated successfully at six other sites in all seasons. In all studies involving commercial greenhouses, the mean absolute error (MAE) between the measured and simulated air temperatures was less than 2 °C, while the MAE for the RH was less than 8% [20]. For many greenhouses studied with the model, the MAE for air temperature and the RH were less than 1 °C and 4% [20]. One limitation with environmental data collected from commercial greenhouses is that the sensor calibration history is not usually available to the research team.

There are several advantages to the model used in this study compared with others in the literature [13,17,21]. As mentioned earlier, the model has been validated in each climatic season at seven unique greenhouses, ranging greatly in complexity and site properties. Most literature models are validated for a short duration at one site, leading to uncertainty about the model accuracy in other seasons and at different locations. Another advantage is that the current model can account for the environmental control technology common at commercial greenhouses in Ontario, such as evaporative cooling pads, supplemental heating and lighting, plant evapotranspiration, dehumidification technology, and curtains.

Figure 2 shows the heat transfer pathways considered in the model with the energy curtain at the site deployed. Corresponding equations are given in Appendix A (slightly different pathways exist when the curtain is not in use), and each heat transfer term can be seen in the nomenclature table in Appendix C. An energy and mass balance are performed at each time step (six seconds) to find the changes in the temperature and absolute humidity. The equations used to find the temperature change of each layer, and the absolute humidity change of the indoor air, can be seen in the Appendix A. Table 2 lists the properties used in the model, which were obtained from multiple sources [21–25]. The solar transmissivity and reflectivity vary based on the solar elevation angle (Table 2).

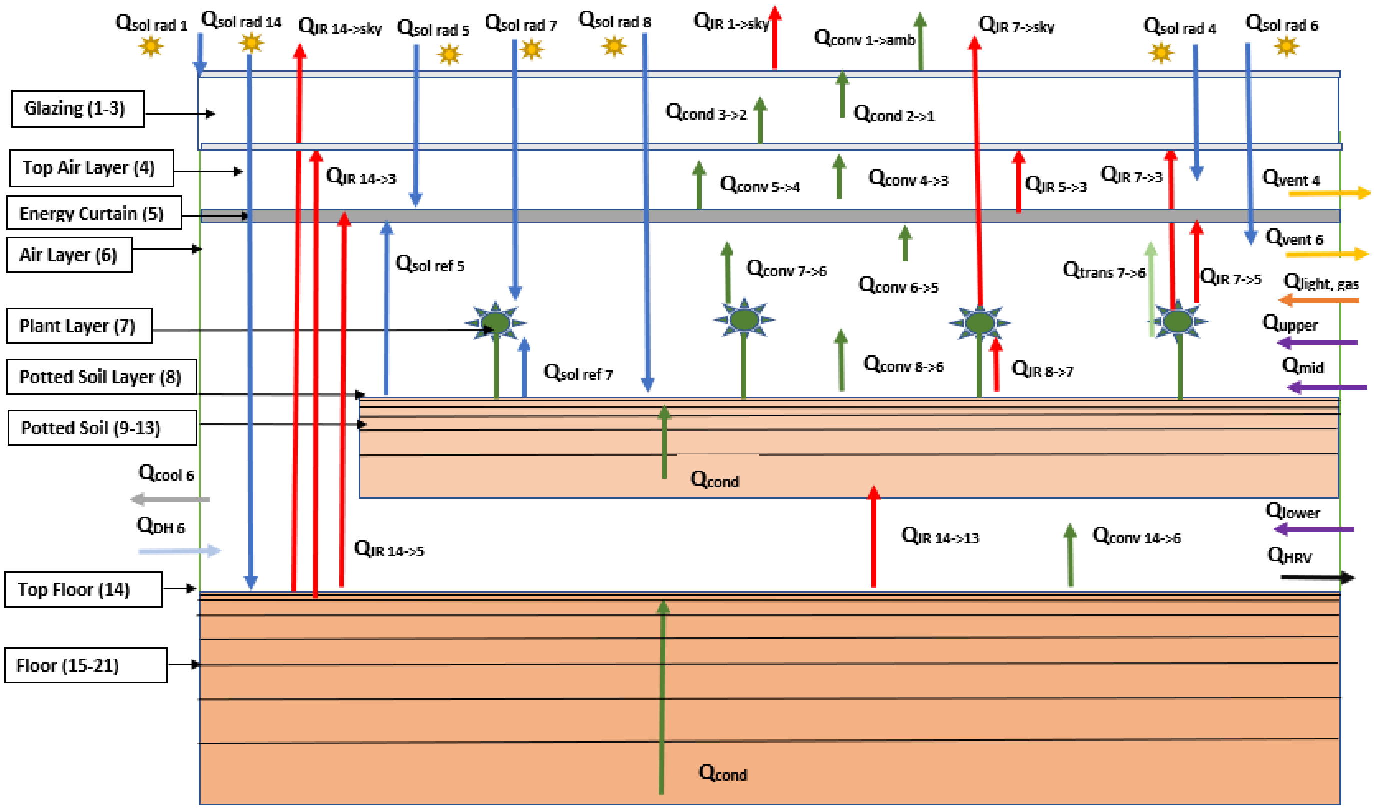

Figure 2. Model layers and heat transfer pathways. Arrows point in positive directions.

Table 2. Summary of parameters used in the model.

Parameter	Value	Variable	Parameter	Value	Variable
Glazing IR transmissivity	0.1	$\tau_{IR,\,1}$	Floor thermal conductivity (W·m^{-1}·K^{-1})	1.9	$k_{14\text{–}21}$
Glazing solar radiation reflectivity	0.21–0.5	$\alpha_{sol\ 1}$	Floor heat capacity (J·kg^{-1}·K^{-1})	880	$c_{14\text{–}21}$
Glazing solar radiation transmissivity	0.48–0.77	$\tau_{sol,\,1}$	Floor and soil IR emissivity	1.0	$\varepsilon_{IR,\,8,14}$
Glazing heat capacity (J kg^{-1}·K^{-1})	2500	c_1	Air heat capacity (J·kg^{-1}·K^{-1})	1007	$c_{2,\,4,6}$
Glazing density (kg·m^{-3})	905	ρ_1	Air density (kg·m^{-3})	1.16	$\rho_{2,\,4,6}$
Glazing thermal conductivity (W·m^{-1}·K^{-1})	0.45	k_1	Air thermal conductivity (W·m^{-1}·K^{-1})	0.0263	$k_{2,4,6}$
Curtain density (kg·m^{-3})	300	ρ_5	Thermal conductivity of potting soil (W·m^{-1}·K^{-1})	1.25	$k_{8\text{–}13}$
Soil and floor solar radiation reflectivity	0.5	$\alpha_{sol\ 8,\,14}$	Plant solar radiation reflectivity	0.16	$\alpha_{sol\ 7}$
Floor density (kg·m^{-3})	2300	$\rho_{14\text{–}21}$	Plant IR emissivity	0.9	$\varepsilon_{IR,\,7}$
Plant density (kg·m^{-3})	1421	ρ_7	Plant heat capacity (J·kg^{-1}·K^{-1})	4180	c_7
Curtain specific heat capacity (J·kg^{-1}·K^{-1})	1800	c_5	Curtain solar radiation reflectivity	0.07	$\alpha_{sol\ 5}$
Curtain solar radiation transmissivity	0.88	$\tau_{sol,\,5}$	IR transmissivity of curtain	0.1	$\tau_{IR,\,5}$
Curtain IR emissivity	0.5	$\varepsilon_{IR,5}$	Glazing IR emissivity	0.9	$\varepsilon_{IR,\,1}$
Curtain IR reflectivity	0.07	$\alpha_{IR,\,5}$	Glazing IR reflectivity	0.07	$\alpha_{IR,\,1}$
Density potting soil (kg·m^{-3})	1300	$\rho_{8\text{–}13}$	Potting soil specific heat capacity (J·kg^{-1}·K^{-1})	1350	$c_{8\text{–}13}$

2.3. Model Controller Configuration

A controller was modelled to realistically set the supplemental heating, lighting, ventilation, curtain, and dehumidification use based on the air temperature and RH setpoints. The CO_2 burners were assumed to run during the daytime in the winter. The upper and lower air temperature setpoints were 21 °C and 25 °C, while the RH setpoints were 65% and 85%. Outside weather data was from an hourly typical meteorological year (TMY) file for Vinland, Ontario [26]. If the simulated indoor air temperature was above or below the setpoint range, the amount of heat per unit floor area to be provided or removed was

$$\Delta Q = \begin{cases} \frac{(T_{air} - 25\ °C)\ c_p\ \rho_{air}\ V_{GH}}{dt\ A_{GH}} & T > 25\ °C \\ \frac{(21\ °C - T_{air})\ c_p\ \rho_{air}\ V_{GH}}{dt\ A_{GH}} & T < 21\ °C \end{cases} \tag{1}$$

where T_{air} represents the air temperature, in °C; ρ_{air} represents the density of the air, in kg·m^{-3}; c_p is the specific heat capacity of the air, in J·kg^{-1}·K^{-1}; dt is the time step, in seconds; and V_{GH} and A_{GH} are the volume and surface area of the greenhouse, in m^3 and m^2, respectively. Each of the three greenhouse heating pipes was capable of providing up to 80 W·m^{-2} of heat. When the air temperature was below the minimum set point, it was ensured that the amount of heat being supplied by the heating pipes was at least the value calculated in Equation (1).

When the air temperature was too high, the exhaust fans were utilized, assuming the amount of cooling from a single fan was

$$Q_{fan} = \left(\frac{f}{V_{GH}}\right) dx\ c_p\ \rho_{air}(T_{air} - T_{outside}) \tag{2}$$

where f is the fan flow rate, in m^3·s^{-1}; dx is the vertical thickness of the air layer, in m; and $T_{outside}$ is the outdoor air temperature, in °C.

A dynamic energy balance (DEB) was performed to help minimize the amount of time the air temperature was outside the setpoint range, by calculating the difference between the heat entering and exiting the greenhouse envelope, in W·m^{-2}. The heat entering the greenhouse came from solar radiation, supplemental heating and lighting, and dehumidification operation, while the heat exiting the greenhouse consisted of the ventilation and leakage heat loss, the infrared (IR) heat lost between the greenhouse components and the sky, the convective heat transfer from the glazing to the ambient air, and the heat used for crop evapotranspiration. The amount of heating and ventilation required when the temperature was within the setpoints was then based on the magnitude of the net energy entering or leaving the greenhouse.

If the RH was too high, ventilation and/or supplemental heating was provided, while the heating and/or ventilation was decreased when the RH was too low. For test cases involving the dehumidification units, the dehumidifiers were run if the RH was above 64%.

The latent heat of condensation (for the MRD and LDD units) and sensible waste heat were released into the greenhouse when dehumidifiers were operating. The total heat input was

$$Q_{DH}\left(\frac{W}{m^2}\right) = \frac{\left(0.9\ DH_{power} + \lambda\ 1000\ \dot{M}\right)}{A_{GH}} \tag{3}$$

where DH_{power} is the electrical consumption of the unit, in W; λ is the latent heat of condensation (2500 J·g^{-1}); and $\dot{M}$ is the mass of water removed by the unit every second, in kg·s^{-1}. It was assumed 90% of the electrical input was released as sensible heat [6]. The HRV did not condense the water vapor, so only its electrical power was considered in Equation (3).

2.4. Model Controller Logic

Table 3 summarizes the simulated controller logic. The logic for the HRV system varied slightly, with air exchange occurring between the indoor and outdoor air, while the MRD and LDD units condensed the moisture directly in the greenhouse. It was assumed the supplemental lights (HPS or LED) were turned off from 12:00 a.m. to 2:00 a.m. every night, and then ran until the target daily light interval (DLI) of 15 mol PAR·m^{-2}·d^{-1} was reached. In Table 3, ΔQ_{i-1} represents the supplemental heat supplied at the previous data time step, which is multiplied by a fraction, d (0–1) depending on the dynamic energy balance (*DEB*) result at each time step and the simulated RH value. If excessive energy was entering the greenhouse envelope, but temperature was still within the setpoints, an appropriate number of exhaust fans were deployed. This prevented rapid oscillations in the simulated air temperature and RH values. With the dehumidifiers running, less ventilation was required to manage the humidity. The simulated air temperature took precedence over the simulated RH when determining the heating and venting schedules.

Table 3. Controller logic with dehumidifier in use.

Temperature	RH	Supplemental Heat	Ventilation	Dehumidification
Above setpoint	Above setpoint	None	Equations (1) and (2)	ON
Within setpoints	Above setpoint	ΔQ_{i-1} d	DEB	ON
Within setpoints	Below setpoint	ΔQ_{i-1} d	DEB	OFF
Below setpoint	Above setpoint	Equation (1)	None	ON
Above setpoint	Below setpoint	None	Equations (1) and (2)	OFF
Above setpoint	Within setpoints	None	Equations (1) and (2)	ON
Below setpoint	Below setpoint	Equation (1)	None	OFF
Below setpoint	Within setpoints	Equation (1)	None	ON
Within setpoints	Within setpoints	ΔQ_{i-1} d	DEB	ON

2.5. Dehumidification Model

Constant power consumption was assumed for the three dehumidification units based on analyzing the site data, and the moisture removal rates for the MRD and LDD were assumed as constant. The HRV moisture removal rate depends on indoor and outdoor conditions and required calculations at each time step. Table 4 shows a summary of the power consumption and moisture removal rates of the three units from the measured data. Each of the three dehumidification units can be seen in Appendix D, along with schematics showing the components and processes.

Table 4. Summary of dehumidification units (n is number of data points available).

Unit	n	Unit Power (kW)	Uncertainty (+/− kW)	Moisture Removal Rate (kg·hr^{-1})	Uncertainty (+/− kg·hr^{-1})
MRD	1934	10.00 (electrical)	1.64	35.80	6.32
LDD	614	2.40 (electrical) 18.9 (hot water)	0.28 3.20	12.96	1.80
HRV	673	0.780 (electrical)	0.036	N/A	N/A

The temperature ratio η_{HRV} of HRV systems (in %) can be defined as [27]

$$\eta_{HRV} = 100\% \times \left(\frac{T_{supply} - T_{outside}}{T_{inside} - T_{outside}} \right) \tag{4}$$

where T_{supply} is the temperature of air leaving the unit and entering the greenhouse. The measured temperature ratio typically varied between 30% and 60%. The temperature ratio was modeled as a linear relationship based on the fit to the temperature difference between the indoor and outdoor air taken from measured data shown in Figure 3.

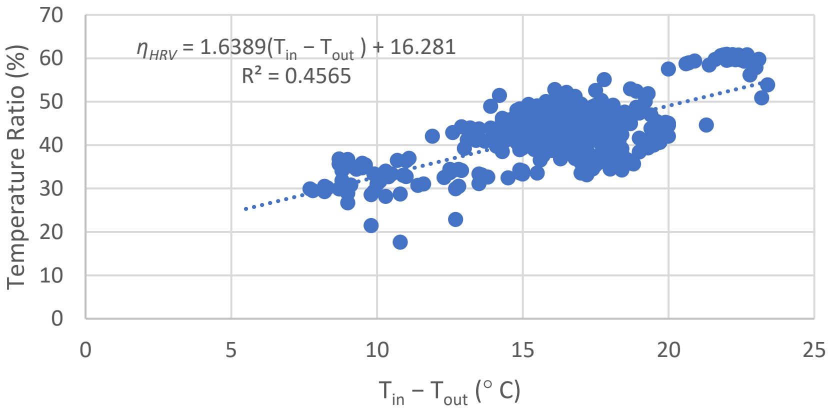

Figure 3. HRV temperature ratio based on indoor and outdoor temperatures.

The supply air temperature could then be approximated using Equation (4). The amount of sensible heat transfer from the HRV could then be found using the flow rate, f_{HRV}, which was assumed to be constant at 2.4 m^3·s^{-1} based on experimental values:

$$Q_{HRV} = \frac{f_{HRV}\,\rho_{air}\,c_p\left(T_{inside} - T_{supply}\right)}{A_{GH}} \tag{5}$$

The value of Q_{HRV} was then subtracted from the air layer energy balance at each time step, shown in Equation (A5) in Appendix A.

The specific humidity (kg moisture/kg dry air) of the inside air and the air entering the greenhouse are required to find the amount of moisture removed by running the HRV. The specific humidity of the indoor air (q_{in}; mass of moisture over mass of dry air) is found using the atmospheric pressure P [28].

$$q_{in} = \frac{0.622\,e}{P - e\,(1 - 0.622)} \tag{6}$$

The vapor pressure e, in Pa, is [29],

$$e = 610.94\left(\frac{RH_{in}}{100\%}\right) e^{\frac{17.625+T_{in}}{243.04+T_{in}}} \tag{7}$$

where T_{in} is the indoor temperature, in °C. The moisture removal rate is then:

$$\dot{M} = f_{HRV}\,\left(q_{in}\rho_{in} - q_{supply}\rho_{supply}\right) \tag{8}$$

where q_{supply} and ρ_{supply} are the specific humidity and density of the supply air. An empirical relationship was derived to calculate the specific humidity of the air leaving the HRV and entering the greenhouse. Ideally, the specific humidity of the supply air would equal the outside air specific humidity, but the system leakage would mean this was not always the case. An empirical linear fit of the measured outdoor specific humidity versus the supply air specific humidity was used:

$$q_{supply} = 0.605\,q_{outside} + 0.0054 \tag{9}$$

2.6. Lighting Model

The DLI target was set to 15 mol PAR·m^{-2}·d^{-1} at the canopy level based on information from the grower. The solar radiation entering the greenhouse envelope and reaching the crop canopy was converted from units of W·m^{-2} (G) to µmol PAR·m^{-2}·s^{-1} using an empirical equation derived by the researchers, and seen below, where $\tau_{glazing}$ is the solar transmissivity of the glazing, and lux and foot-candle are the units of illuminance [30,31].

$$L_{sol}\left(\frac{\mu mol\ PAR}{m^2\ s^1}\right) = \left(\left(122\ \tau_{glazing}\ G + 50\right)\left(\frac{lux}{\frac{W}{m^2}}\right)\right)\left(\frac{foot - candle}{10.76 lux}\right)\left(\frac{0.20\ \frac{\mu mol\ PAR}{m^2\ s^1}}{foot - candle}\right) \tag{10}$$

The site includes 120 HPS lamps in Section A (which is used for the lighting simulations) that deliver approximately 85 µmol PAR·m^{-2}·s^{-1}. For continuity, this value was maintained when simulating the LED test cases by changing the assumed number of light fixtures to maintain this intensity. Table 5 gives details of the two commercially available LED lights included in the analysis [32]. This information was taken from a database reporting grow light experimental test results, which often differ from manufacturer-reported values [32].

Table 5. Properties of HPS and LED lights used in model.

Lighting	Lighting Model	Efficacy (µmol PAR·J^{-1})	Photosynthetic Photon Flux (µmol PAR·s^{-1})	Electrical Input Power (W)	Number of Fixtures Required
LED A	GLPI630HU660D11	4.06	2436	600	47
LED B	SPS 640-GL1	2.80	1745	626	66
HPS	HPS (Existing)	1.60	950	600	120

The color spectrum intensity of the LED lights considered in the study are known, and are shown in Table A1 of Appendix B. While the exact lighting recipe for the existing HPS lights is not directly known, it is typical for HPS lights to emit light in the red and green spectrum (not much in the blue spectrum). This spectrum can be characterized as having a color temperature of 3500 K to 4500 K and being a warm white in appearance.

It is widely recognized that using HPS lamps reduces the greenhouse heating load compared with LED lights. This is partly because LEDs are more efficient, so the same photon flux is delivered with less electrical power than HPS lamps, and partly because the radiant heat (FIR and NIR) emitted by HPS lamps is reflected downwards towards the crop canopy, resulting in higher crop temperatures than LEDs [17,33]. In the model, the electrical input to LED lights was partitioned into convective (26%), radiative (27%), and PAR light (47%) energy outputs, while for HPS lights the energy output was 11% convective, 55% radiative, and 34% PAR light [33]. These values are similar to those used by [17], with one main difference being that no convective cooling was assumed to occur in LED lights. For HPS lamps, the radiative heat component (FIR and NIR) was added to the solar irradiance reaching the crop canopy and floor layers, while for LEDs, the radiative component was assumed to be released to the air [33]. In both HPS and LED test cases, the convective proportion was released to the air layer, while the bulk of the PAR light flux (88%) was added to the crop layer as a heat transfer term, with 3% converted to biomass, and the remainder being reflected and leaving the greenhouse [15].

3. Results

3.1. Controller Validation

Simulations using the controller were tested against the measured data with and without the dehumidifiers in use. The root mean squared error (RMSE) and the mean absolute error (MAE) between the simulated and measured results were calculated for the air temperature, absolute humidity, and RH. The amount of input energy predicted was compared with the actual energy use recorded in the data. Each test case was a week in duration. The natural gas used by CO_2 burners was included in the analysis.

Figure 4 shows the simulated versus the measured air temperature and absolute humidity with the MRD running in the winter as an example. Table 6 summarizes the validation results for all six test cases, including the predicted and measured energy consumption values (in kWh) for natural gas and electricity. The percentage difference between the simulated and measured electrical energy consumption ranged from 5.28% to 6.49%, while the differences for natural gas ranged from 0.85% to 4.61%. The simulated RH never exceeded 95%, and rarely exceeded 90%. Figure 4 shows that the simulated absolute humidity values drop each night at midnight, which is due to the HPS lights being turned off for two hours. In the measured data, the lights were on all night, and were occasionally turned off during the day, suggesting a reason for the discrepancy between the absolute humidity measurements and simulations.

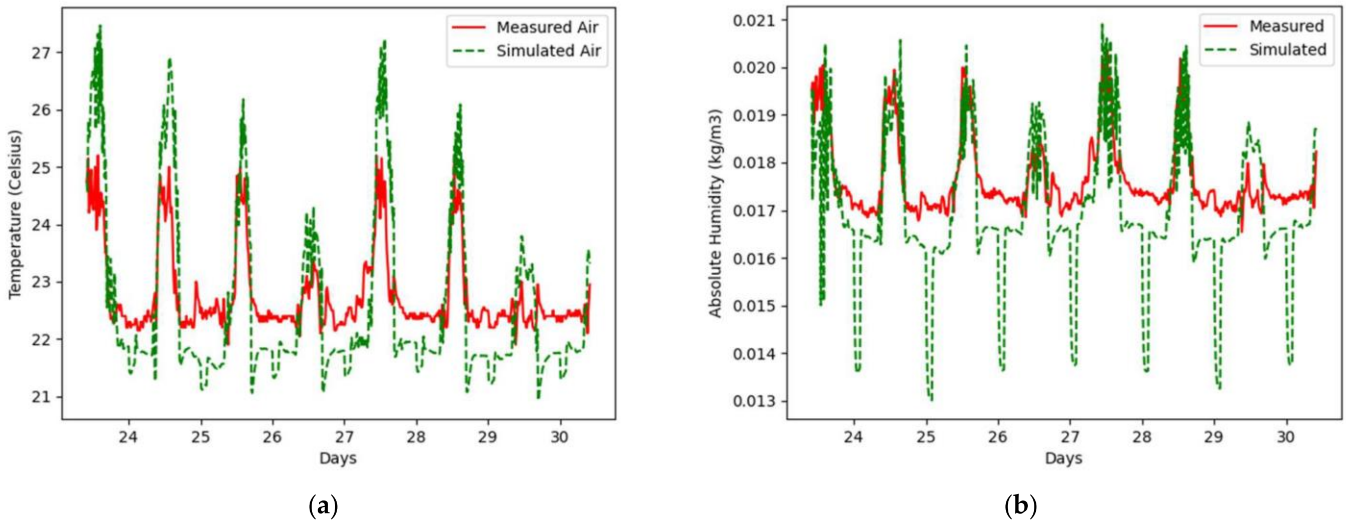

Figure 4. Simulated versus measured values with MRD running: (**a**) air temperature—MRD running, 23–30 December 2019 and (**b**) absolute humidity of air—MRD running, 23–30 December 2019.

Table 6. Results of validation test cases. Percent difference shown in parentheses.

Case	Electrical Consumption (kWh)	Natural Gas Consumption (kWh)	RMSE Air Temperature (°C)	MAE Air Temperature (°C)	RMSE RH (%)	MAE RH (%)	RMSE AH (kg·m^{-3})	MAE AH (kg·m^{-3})
MRD on (12/23/2019 to 12/30/2019)	Data = 12.119 Model = 12.777 (5.28%)	Data = 13.136 Model = 12.925 (1.62%)	0.95	0.81	5.28	2.95	0.0013	0.0010
MRD off (12/31/2019 to 1/6/2020)	Data = 11.867 Model = 11.121 (6.49%)	Data = 24.209 Model = 24.955 (3.03%)	0.76	0.55	4.71	3.57	0.0010	0.0007
LDD on (12/23/2019 to 12/30/2019)	Data = 10.802 Model = 11.505 (6.30%)	Data = 16.499 Model = 15.755 (4.61%)	1.03	0.89	4.35	3.05	0.0011	0.0008
LDD off (12/31/2019 to 1/6/2020)	Data = 11.864 Model = 11.120 (6.47%)	Data = 20.506 Model = 20.757 (1.22%)	0.74	0.56	4.19	3.01	0.0011	0.0009
HRV on (12/23/2019 to 12/30/2019)	Data = 10.510 Model = 11.184 (6.21%)	Data = 31.445 Model = 30.433 (3.27%)	1.14	0.83	4.46	3.25	0.0013	0.0010
HRV off (12/31/2019 to 1/6/2020)	Data = 11.852 Model = 11.143 (6.17%)	Data = 33.204 Model = 33.486 (0.85%)	1.02	0.69	4.98	3.91	0.0015	0.0011

3.2. MRD Results

The TMY data was used for the spring, fall, and winter to run test cases with and without the MRD in use at Section A. The summer was neglected due to the high ventilation requirement for temperature control. As mentioned above, it was assumed that the MRD removed 35.80 L·hr^{-1} of the moisture from the air and consumed 10 kW of electricity. Table 7 summarizes the energy results, along with a range of possible savings ($CAD), and an estimate of CO_2 emissions (kg CO_{2e}). Two electrical rate constants were used (0.055 $\cdot$kWh^{-1} and 0.127 $\cdot$kWh^{-1}), which were obtained from discussions with growers. A range of natural gas prices was used based on the typical rates, with \$4.80$\cdot$GJ^{-1}, \$10.00$\cdot$GJ^{-1}, and \$14.00$\cdot$GJ^{-1} considered [34]. The carbon intensity in g $CO_{2e}\cdot$kWh^{-1} for the natural gas and electricity in Ontario was assumed to be 181 and 53, respectively [35].

Table 7. Summary of MRD results.

Season	MRD Status	Electrical Energy Consumption (kWh)	Natural Gas Energy Consumption (kWh)	kg CO_{2e}	Energy Saved with MRD in Use (kWh)	Range of Savings (\$CAD)
WINTER	On off	132.389 112.733	238.234 325.295	50.137 64.853	67.405 (15.4%)	−990 to 3272
FALL	on off	135.177 115.314	126.931 225.448	30.139 46.918	78.654 (23.1%)	−818 to 3833
SPRING	on OFF	95.080 78.114	64.345 130.957	16.686 27.843	49.646 (23.8%)	−1002 to 2397

Running the MRD saved energy (the sum of electrical and natural gas) in each season tested compared with the non-use cases, due to the reduction in the sensible heat loss and the capture of latent heat. Cost savings depend heavily on natural gas and electricity rates, with the cheaper electricity and expensive natural gas resulting in larger savings. Figure 5 shows the cost of removing 1 L of moisture with the MRD or with one exhaust fan during one week in winter using two sets of electricity and natural gas rates. It was assumed that the heat lost from running the exhaust fan was entirely from the supplemental heating (i.e., natural gas), when in reality, some of it would be from solar radiation or waste heat from the HPS lamps. Thus, when calculating the cost to remove one liter of water vapor from the greenhouse air using an exhaust fan, natural gas rates were used instead of electrical. It costs more to remove 1 L of moisture with the MRD compared to an exhaust fan when electricity rates are high, but this reverses when the lower rate is used. This means that the feasibility of implementing the MRD at a particular greenhouse is highly dependent on the energy rates paid by the grower.

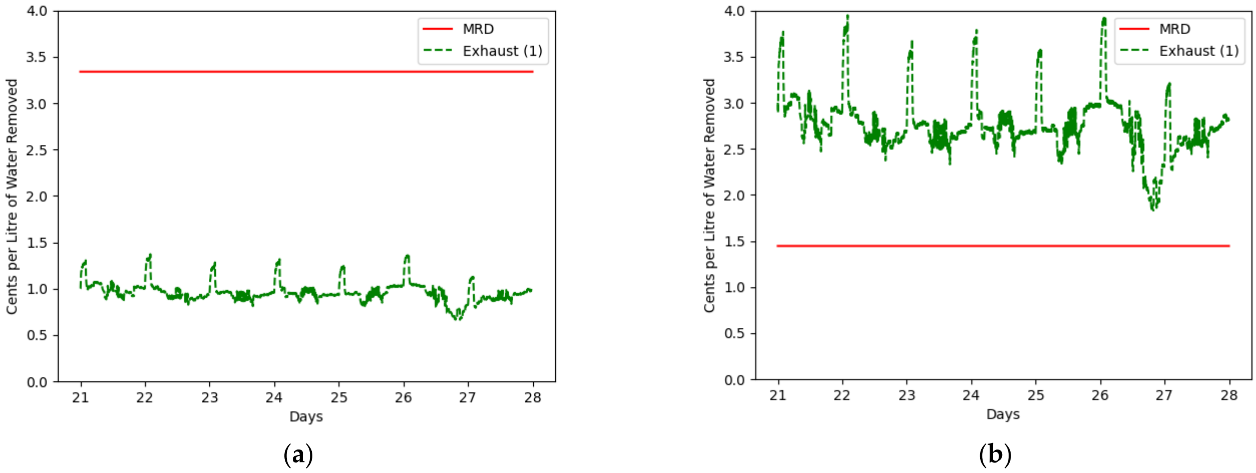

Figure 5. MRD and exhaust fan cost comparison in winter (21–28 December) assuming energy costs of (**a**) \$4.80/GJ for gas, \$0.127 \$/kWh for electricity, and (**b**) \$14.00/GJ for gas, \$0.055 \$/kWh for electricity.

A comparison was made to experimental data collected from the site during the early spring conditions [36] (Table 8). In the comparative study [36], the authors conducted ON/OFF trials for two weeks with the dehumidification units (MRD, LDD, HRV). However, a larger seasonal analysis was not performed. It is impossible to experimentally measure the energy savings from running the MRD versus not running the MRD at a particular greenhouse bay at the same time, with the same weather conditions. This adds to the value of accurate, validated simulations, which can simulate the same external weather and site conditions with and without the unit running.

Table 8. Comparison between experimental data and simulation results for MRD spring test case.

	MRD Status	Average RH (%)	Unit Power (kWh)	Heat (kWh)
12–26 March 2019 [36]	ON	78.2	1450	15.024
	OFF	81.3	N/A	20.267
	Savings (%)	N/A	N/A	25.9
20–27 March TMY Current Study	ON	75.9	1464	11.102
	OFF	77.6	N/A	17.852
	Savings (%)	N/A	N/A	37.8

Table 8 shows that the MRD use can reduce the average indoor RH by 1–3% and reduce heating energy requirements due to the decreased ventilation. The simulation results showed a higher reduction in heating energy with the unit running than the experimental results. This can be partly attributed to the outdoor air temperature being warmer with the unit off (2.8 °C) than with the unit on (1.9 °C).

When installing an MRD, it must be properly sized for the greenhouse, and should be placed in the middle of the greenhouse to promote uniform temperature and humidity profiles [1]. As these units directly condense water in the greenhouse, they contribute both sensible and latent heat to the greenhouse environment. In the warmer weather, when high rates of ventilation are required for temperature control, the units are typically not run, as the treated air would be quickly removed through ventilation. As such, the spring, fall, and winter are the optimal seasons to operate the units in the southern Ontario context.

3.3. LDD Results

Table 9 shows the LDD results. While smaller energy savings were predicted with the LDD compared with the MRD, the lower electrical consumption of the LDD unit resulted in a decreased likelihood that negative cost savings would occur due to the high electricity rates. In all three seasons, it was found that running the LDD saved both energy and cost. The natural gas energy usage includes the heat energy required to regenerate the desiccant solution.

Table 9. Summary of LDD results.

Season	LDD Status	Electrical Energy Consumption (kWh)	Natural Gas Energy Consumption (kWh)	kg CO_{2e}	Energy Saved with LDD in Use (kWh)	Range of Savings ($CAD)
WINTER	ON	117.393	246.110	50.768	43.179 (10.6%)	234 to 2136
	OFF	112.720	293.962	59.181		
FALL	ON	119.929	139.170	31.546	55.068 (17.5%)	444 to 2730
	OFF	115.293	198.873	42.107		
SPRING	ON	81.875	76.629	18.209	31.971 (16.8%)	121 to 1579
	OFF	77.932	112.543	24.501		

To illustrate the seasonal effect on the ventilation efficiency, a comparison between the early winter and early fall was performed (Figure 6). The amount of moisture that can be removed by the exhaust fans is higher in the winter when humidity differences between the indoor and outdoor air are greater.

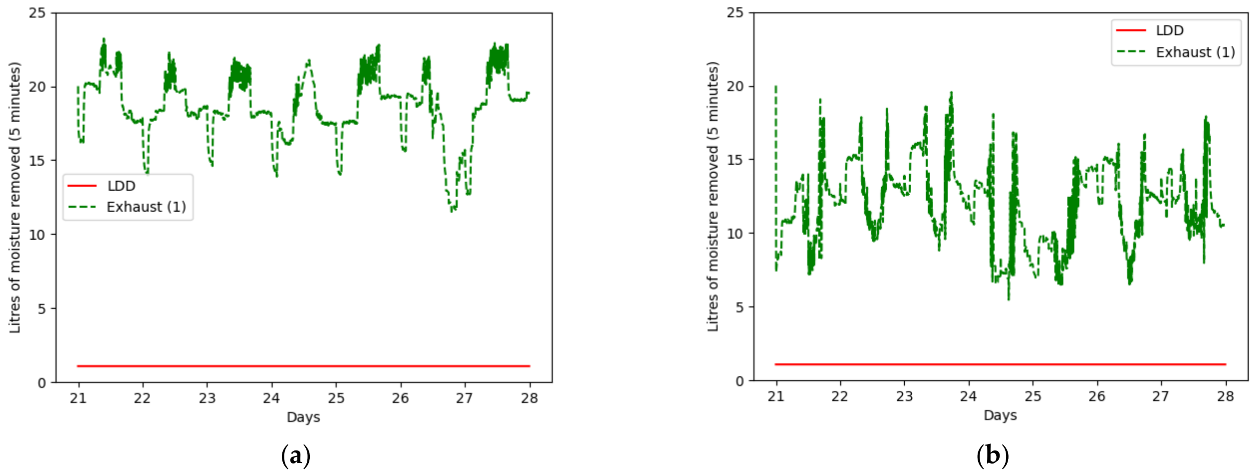

Figure 6. Moisture removal capacity, in units of liters per five-minute period, of LDD and exhaust fan in (**a**) winter (21–28 December) and (**b**) fall (22–29 September) conditions.

Table 10 shows a comparison of the measured data [36] and simulation results for the LDD. An excellent correlation is apparent between the simulations and measured data. The magnitude of the heat energy reduction using the LDD matched well with the measured data, as did the overall LDD power consumption.

Table 10. Comparison between experimental data and simulation results for LDD spring test case.

	MRD Status	Average RH (%)	Unit Electrical Energy (kWh)	Unit Regeneration Energy (kWh)	Heat (kWh)
12–26 March 2019 [36]	ON OFF Savings (%)	84.3 87.7 N/A	368 N/A N/A	3070 N/A N/A	14.801 20.136 26.5
20–27 March TMY Current Study	ON OFF Savings (%)	77.7 78.9 N/A	357 N/A N/A	2818 N/A N/A	11.201 15.609 28.2

Similar to the MRD, the LDD should be placed in the middle of the greenhouse for optimal performance. However, the LDD unit requires heat (typically delivered via hot water pipes) to regenerate the desiccant solution, which could complicate its placement in the greenhouse. The solar-driven regeneration of the desiccant solution has been examined in recent years, but the intermittent nature of solar radiation is a limitation in the widespread application [37]. As with the MRD, the unit is typically not operated in summer conditions, due to the high rate of ventilation for the temperature control.

3.4. HRV Results

Table 11 shows simulation results for the HRV test cases. As the HRV consumed the least electricity of the three units (0.78 kW), the difference in the electrical consumption between the HRV on and off was the lowest of the three technologies. This resulted in cost savings in every scenario. Since the temperature efficiency ratio is less than 1.0, colder air was introduced into the greenhouse when the HRV was operating, which increased heating loads compared to the MRD and LDD units and resulted in lower CO_{2e} reductions. In addition, it is notable that the greenhouse bay with the HRV unit (Section C) had a surface area that was 33% greater than the bays with the MRD and LDD, resulting in higher total heating requirements. Note that the winter, fall, and spring in Tables 7, 9 and 11 correspond to 21 December to 19 March, 22 September to 20 December, and 20 March to 20 June. In Tables 7, 9 and 11, the natural gas energy refers to the energy required for space heating (and desiccant regeneration for the LDD), while the electrical energy is the amount of energy required to operate the supplemental lights, exhaust fans, and dehumidification units.

Table 11. Summary of HRV results.

Season	HRV Status	Electrical Energy Consumption (kWh)	Natural Gas Energy Consumption (kWh)	kg CO_{2e}	Energy Saved with HRV in Use (kWh)	Range of Savings ($CAD)
WINTER	On off	102.158 101.908	430.274 451.970	83.294 87.208	21.446 (3.87%)	344 to 1071
FALL	on off	104.867 104.612	279.102 283.406	56.075 56.841	4048 (1.04%)	42 to 201
SPRING	on OFF	73.521 73.240	115.576 120.320	24.816 25.660	4463 (2.31%)	46 to 222

Table 12 shows controller simulations compared with the corresponding measured data [36]. Both the simulation results and measured data showed a relatively small decrease in the heating energy when using the HRV unit, while the measured data showed that the average RH was higher when the unit was on than when it was off.

Table 12. Comparison between experimental data and simulation results for HRV spring test case.

	MRD Status	Average RH (%)	Unit Power (kWh)	Heat (kWh)
12–26 March 2019 [36]	ON OFF Savings (%)	76.1 70.8 N/A	131 N/A N/A	28.002 28.465 1.6
20–27 March TMY Current Study	ON OFF Savings (%)	70.3 70.2 N/A	45 N/A N/A	20.614 21.183 2.7

The effectiveness of an HRV is highly dependent on the outdoor weather conditions. When the ambient outdoor air is hot and humid, the system cannot adequately dehumidify the greenhouse [9]. During the wintertime, colder air may be introduced to the greenhouse, as the sensible heat recovery efficiency is not 100%. While the electrical energy required to operate the HRV was the lowest of the three units considered, it also had the smallest impact on reducing the energy consumption. Altering the controller logic could possibly improve the results and is worth exploring in greater detail in future work. In general, the optimal seasons for the use of HRV systems are the shoulder months in the spring and fall [9]. Installing an HRV unit typically requires additional duct work for incoming and outgoing air pathways. As the unit does not condense water vapor directly inside the greenhouse, the latent heat is lost from the greenhouse through ventilation. As with the MRD and LDD systems, the unit should be properly sized for the greenhouse, with a suggested moisture removal rate of 0.018 $L{\cdot}hr^{-1}{\cdot}m^{-2}$ for cool periods in the Canadian Prairies [9].

3.5. Lighting Results

The TMY data from each season (spring, summer, fall, and winter) were simulated for the LED and HPS light scenarios. Similar to the sections above, the amount of energy required for heating and for electricity (lights, exhaust fans) was tracked and is presented in Table 13. The dehumidification equipment was assumed to be turned off for these simulations, and the evaporative cooling pads were only included in the summer simulations. The amount of heating required is higher for the LED test cases in each season than for the HPS cases, as expected. In both the fall and winter, the LED test cases required more total energy than the corresponding HPS test cases, due to the higher heating demand.

However, since electricity is more expensive than natural gas on a unit energy basis, cost savings were possible in every season.

Table 13. Summary of lighting simulation results.

Season	Light Type	Electrical Energy Consumption (kWh)	Natural Gas Energy Consumption (kWh)	kg CO_{2e}	Energy Saved Relative to Baseline HPS Use (kWh)	Range of Savings ($CAD)
	HPS	108.378	274.780	55.479	N/A	N/A
WINTER	LED A	43.325	355.728	66.683	−15.895	−469 to 6861
	LED B	61.905	336.522	64 191	−15.269	−531 to 4834
	HPS	111.091	171.864	36.995	N/A	N/A
FALL	LED A	44.905	238.385	45.528	−335	314 to 7255
	LED B	64.054	222.597	43.685	−3696	50 to 5096
	HPS	74.863	102.496	22.520	N/A	N/A
SPRING	LED A	31.634	122.597	23.867	23.127	1372 to 5142
	LED B	44.144	118.149	23.725	15.065	907 to 3630
	HPS	75.614	25.055	8542	N/A	N/A
SUMMER	LED A	34.454	31.977	7614	34.234	1918 to 5107
	LED B	46.368	30.575	7992	23.724	1332 to 3618

The presented results do not account for any differences in the product yield or quality that may be influenced by switching to LED lights. Researchers have found higher yields and improved quality comparing LED lighting systems with HPS for cucumber crops [38], which offers the potential for additional financial benefits that are not captured in this study. In addition, it is worth noting that the study greenhouse (growing potted roses) has a lower photosynthetic photon flux density (85 µmol PAR·m^{-2}·s^{-1}) provided by the assimilation lighting than more intensive vegetable or cannabis operations. This means that the findings from this study could be magnified for greenhouses growing crops with a higher DLI requirement.

While the capital cost of investment is often the limiting factor in switching to LEDs at greenhouses in Ontario, incentives are available through programs such as Save on Energy, which can cover up to 50% of the retrofitting costs [39]. LED fixtures also last longer and require less maintenance than HPS lamps [14]. Growers can also use combinations of LED and HPS lamps, which mitigates the higher space heating requirements of switching to LEDs, particularly in the colder seasons. Furthermore, it is worth noting that due to lower crop temperatures with LED lamps, growers often raise the indoor air temperature by 1 °C, which would add to the space heating loads [17].

4. Conclusions

This study suggests good potential for applying the dehumidification technology in southern Ontario greenhouses, with energy savings possible from all three types of dehumidification studied in the winter, spring, and fall conditions. Switching to LED lights from HPS lamps was found to save energy in the spring and summer, with financial savings possible in every season. Major findings include:

1. The results suggest that the best season to run the LDD dehumidification equipment is the fall (17.5% reduction in the overall energy), however, energy savings with the LDD were possible in each season studied and it was profitable in all costing scenarios.
2. The greatest energy savings were found with the MRD in the fall (23.1%). Due to the higher electrical consumption, cost savings were highly dependent on the electricity and natural gas rates.
3. The HRV, with the lowest electrical consumption, was profitable in all costing scenarios, but saved the lowest overall energy of the units studied. It would likely be less effective in summer conditions, as the cost saving effectiveness of the HRV is highly dependent on the humidity difference between indoor and outdoor air [9].

4. Due to the LDD relying on both electricity and natural gas (for regenerating the desiccant solution), the cost effectiveness was less sensitive to the varying natural gas and electricity rates, and it offered strong energy savings potential compared with the baseline of dehumidification by the exhaust fan ventilation.
5. Seasonal carbon emission (kg CO_{2e}) reductions of up to 35.8% were possible with the MRD unit, and significant reductions are also possible with the LDD.
6. Non-operating costs, including capital and maintenance costs associated with each technology, were not quantified nor discussed in this study. With carbon taxes being implemented in Ontario, dehumidification technologies offer a potential pathway for growers to reduce CO_2 emissions, due to the low carbon intensity of the Ontario power grid. Seasonal reductions of up to 16,000 kg CO_{2e} are possible with the MRD, with lower reductions seen with the HRV. With the Canadian federal carbon tax increasing to \$50/tonne CO_{2e} in 2022 [40], a 16,000 kg CO_{2e} reduction corresponds to savings of \$800.
7. At the study greenhouse, switching to LED lamps can save up to \$7,000 in the fall, and up to \$24,300 annually at the studied greenhouse, when higher electricity and lower natural gas rates are used. However, space heating loads increase in each season using LEDs instead of HPSs, and a net increase in the overall energy was found in simulation results for the winter and fall seasons.

Author Contributions: Conceptualization, A.N.; methodology, A.N., J.H., S.H.T. and W.D.L.; software, A.N.; validation, A.N.; formal analysis, A.N.; investigation, A.N.; resources, A.N. and J.H.; data curation, A.N. and J.H.; writing—original draft preparation, A.N.; writing—review and editing, J.H., S.H.T. and W.D.L.; supervision, S.H.T. and W.D.L.; project administration, S.H.T. and W.D.L.; funding acquisition, S.H.T. and W.D.L. All authors have read and agreed to the published version of the manuscript.

Funding: This research was funded by the Ontario Ministry of Agriculture, Food and Rural Affairs (OMAFRA) Alliance—Tier 1 program (grant UG-T1-2020-100103 "Heat Storage to Save Energy in Ontario Greenhouses").

Data Availability Statement: The data presented in this study are available on request from the corresponding author. The data are not publicly available due to requirements to protect commercial interests of the collaborating greenhouse as a condition of data use.

Acknowledgments: The support and assistance of the commercial greenhouse operator Westbrook Greenhouse Systems Ltd. was essential to this study and is gratefully acknowledged.

Conflicts of Interest: The authors declare no conflict of interest. The funders had no role in the design of the study; in the collection, analyses, or interpretation of data; in the writing of the manuscript; or in the decision to publish the results.

Appendix A

In the equations below, dT_i represents the temperature change of each layer at time step dt; with c_i representing the specific heat capacity of the layer in $J{\cdot}kg^{-1}{\cdot}K^{-1}$; ρ_i representing the density of the layer, in $kg{\cdot}m^{-3}$; and dx_i representing the vertical thickness, in m. The heat transfer pathways between layers are a combination of convection (*conv*), conduction (*cond*), evapotranspiration (*trans*), and infrared radiation (*IR*), while the heat resulting from solar input (*sol rad*), heating pipes (*upper, lower, and mid*), CO_2 burner (*gas*), HPS lights (*light*), evaporative cooling pad (*cool*), ventilation (*vent*), and dehumidification (*DH*) inputs are also included. Refer to Figure 2 to see what layer each subscript number corresponds to (i.e., layer 4 is the attic air layer).

$$dT_1 = \frac{dt\left(Q_{sol\ rad_1} + Q_{cond\ 2\to 1} - Q_{conv\ 1\to amb} - Q_{IR\ 1\to sky}\right)}{c_1\,\rho_1\,dx_1} \tag{A1}$$

$$dT_2 = \frac{dt\ \left(-Q_{cond\ 2\to1} + Q_{cond\ 3\to2}\right)}{c_2\ \rho_2\ dx_2} \tag{A2}$$

$$dT_3 = \frac{dt\ \left(Q_{sol\ rad_{ref_3}} + Q_{conv\ 4\to3} + Q_{IR\ 5\to3} + Q_{IR\ 12\to3} - Q_{cond\ 3\to2}\right)}{c_3\ \rho_3\ dx_3} \tag{A3}$$

$$dT_4 = \frac{dt\ \left(-Q_{conv\ 4\to3} + Q_{sol\ rad_4} - Q_{vent_4} + 0.75\ Q_{upper}\right)}{c_4\ \rho_4\ dx_4} \tag{A4}$$

$$dT_6 = \frac{dt\ \left(Q_{sol\ rad_6} + Q_{conv\ 7\to6} + Q_{conv\ 8\to6} - 0.5\ Q_{trans_{7\to6}} + Q_{conv\ 14\to6} - Q_{vent\ 6} - Q_{HRV} + Q_{mid} + 0.25\ Q_{upper} + 0.25\ Q_{lower} + Q_{gas} + Q_{light} - Q_{cool} + Q_{DH}\right)}{c_6\ \rho_6\ dx_6} \tag{A5}$$

$$dT_7 = \frac{dt\ \left(Q_{sol\ rad_7} + Q_{sol\ rad_{ref_7}} - Q_{conv\ 7\to6} - Q_{IR\ 7\to3} + Q_{IR\ 8\to7} - 0.5\ Q_{trans_{7\to6}} - Q_{IR\ 7\to sky} + Q_{light}\right)}{c_7\ \rho_7\ dx_7} \tag{A6}$$

$$dT_8 = \frac{dt\ \left(Q_{sol\ rad_8} - Q_{conv\ 8\to6} - Q_{IR\ 8\to7} + Q_{cond\ 9\to8} + 0.75\ Q_{lower}\right)}{c_8\ \rho_8\ dx_8} \tag{A7}$$

* Note that Equation (A8) is used for layers i = 9 through 12 and i = 15 through 20, with only the layer subscripts changing

$$dT_i = \frac{dt\ \left(Q_{cond\ i+1\to i} - Q_{cond\ i\to i-1}\right)}{c_i\ \rho_i\ dx_i} \tag{A8}$$

$$dT_{13} = \frac{dt\ \left(-Q_{cond\ 13\to12} + Q_{IR14\to13}\right)}{c_{13}\ \rho_{13}\ dx_{13}} \tag{A9}$$

$$dT_{14} = \frac{dt\ \left(Q_{sol\ rad_{14}} - Q_{conv\ 14\to6} - Q_{IR\ 14\to3} + Q_{cond\ 15\to14} - Q_{IR\ 14\to sky} - Q_{IR\ 14\to13}\right)}{c_{14}\ \rho_{14}\ dx_{14}} \tag{A10}$$

$$dT_{21} = \frac{dt\ \left(-Q_{cond\ 21\to20}\right)}{c_{21}\ \rho_{21}\ dx_{21}} \tag{A11}$$

Equations (A12)–(A17) show the modified versions of the equations used when the energy curtain is deployed. These forms of the equation are used instead of the corresponding equation above for dT_i when the energy curtain is deployed and in use.

$$dT_3 = \frac{dt\ \left(Q_{IR5\to3} + Q_{conv\ 4\to3} + Q_{IR\ 7\to3} + Q_{IR\ 14\to3} - Q_{cond3\to2}\right)}{c_3\ \rho_3\ dx_3} \tag{A12}$$

$$dT_4 = \frac{dt\ \left(-Q_{conv\ 4\to3} + Q_{sol\ rad_4} - Q_{vent_4} + Q_{conv\ 5\to4}\right)}{c_4\ \rho_4\ dx_4} \tag{A13}$$

$$dT_5 = \frac{dt\ \left(Q_{sol\ rad_5} + Q_{sol\ rad_{ref_5}} + Q_{conv\ 6\to5} + Q_{IR\ 7\to5} + Q_{IR\ 14\to5} - Q_{conv\ 5\to4} - Q_{IR\ 5\to sky} - Q_{IR\ 5\to3} + 0.75\ Q_{upper}\right)}{c_5\ \rho_5\ dx_5} \tag{A14}$$

$$dT_6 = \frac{dt\ \left(Q_{sol\ rad_6} + Q_{conv\ 7\to6} + Q_{conv\ 8\to6} - 0.5\ Q_{trans_{7\to6}} + Q_{conv\ 14\to6} - Q_{vent\ 6} - Q_{HRV} + Q_{mid} + 0.25\ Q_{upper} + 0.25\ Q_{lower} + Q_{gas} + Q_{light} - Q_{conv\ 6\to5} - Q_{cool} + Q_{DH}\right)}{c_6\ \rho_6\ dx_6} \tag{A15}$$

$$dT_7 = \frac{dt\ \left(Q_{sol\ rad_7} + Q_{sol\ rad_{ref_7}} - Q_{conv\ 7\to6} - Q_{IR\ 7\to3} - Q_{IR\ 7\to5} + Q_{IR\ 8\to7} - 0.5\ Q_{trans_{7\to6}} - Q_{IR\ 7\to sky} + Q_{light}\right)}{c_7\ \rho_7\ dx_7} \tag{A16}$$

$$dT_{14} = \frac{dt\ \left(Q_{sol\ rad_{14}} - Q_{conv\ 14\to6} - Q_{IR\ 14\to3} + Q_{cond\ 15\to14} - Q_{IR\ 14\to sky} - Q_{IR\ 14\to13} - Q_{IR\ 14\to5}\right)}{c_{14}\ \rho_{14}\ dx_{14}} \tag{A17}$$

The variable dAH represents the change in the absolute humidity of the greenhouse air over time step dt, typically in units of kg/m^3. The change is a result of the crop transpiration (*trans*), latent heat transfer from ventilation (*latent*), moisture removed by dehumidification

(*DH*), and moisture added from the CO_2 burner (*gas*). Here, λ represents the latent heat of condensation for water (2500 J·kg^{-1}):

$$dAH = \frac{dt\ (Q_{trans} - Q_{latent})}{\lambda\ dx_{air\ layer}} + M_{gas} - M_{DH} \tag{A18}$$

Appendix B

The color spectrum of the two LED lights used in the analysis can be seen below in Table A1 [32]. Note that the color temperature of the lights is not specified but can be assumed to be around 3000 K to 5000 K (warm white to warm white and blue). As can be seen, one of the LED lights (GLPI630HU660Dll) has most of its color spectrum in the red range, while the other has more of a broad color spectrum (including a significant proportion of blue light).

Table A1. Color spectrum of LED lights used in model [32].

Lighting Model	Photon Flux Blue (400–500 nm)	Photon Flux Green (500–600 nm)	Photon Flux Red (600–700 nm)	Photon Flux Far Red (700–800 nm)
GLPI630HU660D11	0.75 µmol/s	1.62 µmol/s	2433 µmol/s	6.65 µmol/s
SPS 640-GL1	322 µmol/s	734 µmol/s	689 µmol/s	36 µmol/s

Appendix C

Nomenclature used in the text:

A_{GH}	surface area of greenhouse (m^2)
a_{sol}	absorptivity to solar radiation
c	specific heat capacity (J·kg^{-1}·K^{-1})
DH_{power}	electrical consumption of dehumidifier (W)
dAH	change in absolute humidity (kg·m^{-3})
dT	change in temperature (°C)
dt	time step (s)
dx	layer thickness (m)
e	vapor pressure (Pa)
f	exhaust fan flow rate (m^3·s^{-1})
f_{HRV}	ventilation flow rate from HRV (m^3·s^{-1})
k	thermal conductivity (W·m^{-1}·K^{-1})
L_{sol}	PAR light from solar (µmol PAR·m^{-2}·s^{-1})
$\dot{M}$	moisture removed by dehumidifier (kg·s^{-1})
M_{DH}	mass of water removed by dehumidifier (kg moisture·m^{-3})
P	atmospheric pressure (Pa)
Q_{cool}	heat flux from evaporative cooling pad (W·m^{-2})
Q_{cond}	conductive heat flux (W·m^{-2})
Q_{conv}	convective heat flux (W·m^{-2})
Q_{DH}	sensible and latent heat from dehumidifier (W·m^{-2})
Q_{fan}	cooling capacity from single exhaust fan (W·m^{-2})
Q_{gas}	heat flux from CO_2 burner (W·m^{-2})
Q_{HRV}	sensible heat transfer from HRV (W·m^{-2})
Q_{IR}	IR heat flux (W·m^{-2})
Q_{latent}	latent heat loss due to ventilation (W·m^{-2})
Q_{light}	heat flux from HPS/LED lights (W·m^{-2})
Q_{lower}	heat flux lower heating pipe (W·m^{-2})

Q_{mid}	heat flux mid-level heating pipes ($W \cdot m^{-2}$)
$Q_{sol\ rad}$	solar radiation heat flux ($W \cdot m^{-2}$)
$Q_{sol\ rad,\ ref}$	reflected solar radiation heat flux ($W \cdot m^{-2}$)
Q_{trans}	transpiration heat flux ($W \cdot m^{-2}$)
Q_{upper}	heat flux upper heating pipe ($W \cdot m^{-2}$)
Q_{vent}	sensible heat loss due to ventilation ($W \cdot m^{-2}$)
q	specific humidity (kg moisture·kg dry air^{-1})
RH	relative humidity (%)
T	temperature (°C)
V_{GH}	volume of greenhouse (m^3)
α_{IR}	reflectivity to IR radiation
α_{sol}	reflectivity to solar radiation
ε	emissivity to IR radiation
η_{HRV}	temperature efficiency ratio of HRV
λ	latent heat of condensation ($J \cdot g^{-1}$)
ρ	density ($kg \cdot m^{-3}$)
τ_{IR}	transmissivity to IR radiation
τ_{sol}	transmissivity to solar radiation
χ	water vapor concentration ($kg \cdot m^{-3}$)

Appendix D

Appendix D.1. MRD

The MRD considered in this study can be seen below in Figure A1, along with a schematic of the system in Figure A2. This unit is placed inside the greenhouse bay, and takes hot and humid air from the greenhouse, which passes through surfaces that are cooled by the refrigerant to below the dew point temperature. This process condenses the water vapor within the unit, which can be collected and removed or recycled by the grower. The air exiting the unit is hot and dry, as the heat released from condensation can increase the air temperature.

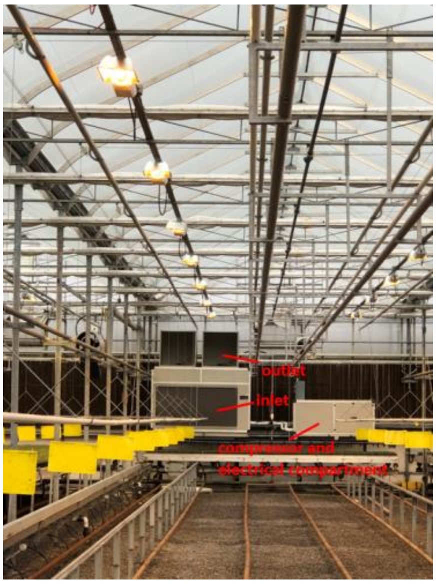

Figure A1. MRD in greenhouse bay.

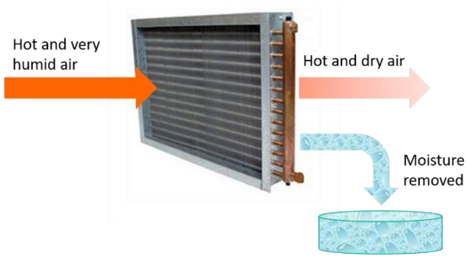

Figure A2. Schematic of MRD functionality.

Appendix D.2. LDD

The LDD dehumidifier considered in this study can be seen below in Figure A3, along with a schematic of the system in Figure A4. In this system, the hot and humid greenhouse air is passed through the unit, which uses a desiccant material to remove the water vapor from the air. When the desiccant material is saturated, it is heated in a recharging cycle, typically by using hot water. The condensed water can be collected and removed, similar to the MRD. The unit is also entirely within the greenhouse, with no interaction with the outside air.

Figure A3. LDD in greenhouse bay.

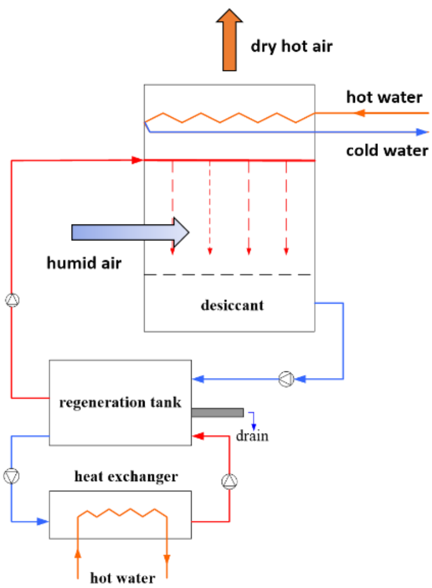

Figure A4. Schematic of LDD functionality.

Appendix D.3. HRV

The HRV dehumidifier considered in this study can be seen below in Figure A5, along with a schematic of the system in Figure A6. This dehumidifier operates by using the outgoing internal greenhouse air to transfer heat to the incoming outdoor air, which is usually drier and colder in the Canadian climate. Although perfect heat transfer is not typically achievable, the system can warm the incoming air by several degrees, reducing the heat lost due to ventilation. As no direct air mixing between the incoming and outgoing air occurs, the incoming air remains dry, and can aid in dehumidifying the greenhouse.

Figure A5. HRV used in study.

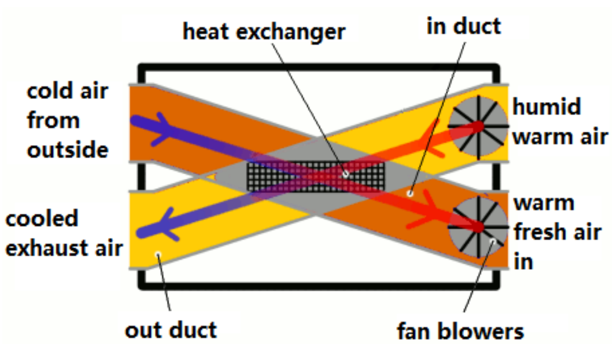

Figure A6. Schematic of HRV functionality.

References

1. Posterity Group. *Greenhouse Energy Profile Study*; Independent Electricity System Operator: Toronto, ON, Canada, 2019.
2. OMAFRA. Greenhouse Industry Statistics, 2012 to 2017. 2019. Available online: http://www.omafra.gov.on.ca/english/stats/hort/greenhouse1.htm (accessed on 31 March 2022).
3. Semple, L.M.; Carriveau, R.; Ting, D.S.-K. Potential for large-scale solar collector system to offset carbon-based heating in the Ontario greenhouse sector. *Int. J. Sustain. Energy* **2018**, *37*, 378–392. [CrossRef]
4. Zheng, Y.; Llewellyn, D.; Dixon, M. *Investigation of the Feasibility to Improve the Lighting Environment under Hanging Baskets in Greenhouse Flower Production*; Flowers Canada Growers: Guelph, ON, Canada, 2013.
5. Amani, M.; Foroushani, S.; Sultan, M.; Bahrami, M. Comprehensive review on dehumidification strategies for agricultural greenhouse applications. *Appl. Therm. Eng.* **2020**, *181*, 115979. [CrossRef]
6. Han, J.; Guo, H.; Brad, R.; Waterer, D. Mechanical Refrigeration Dehumidifier Performance Evaluation in a Tomato Greenhouse in Cold Regions. *Trans. ASABE* **2016**, *59*, 933–941. [CrossRef]
7. Chantoiseau, E.; Migeon, C.; Chasseriaux, G.; Bournet, P.-E. Heat-pump dehumidifier as an efficient device to prevent condensation in horticultural greenhouses. *Biosyst. Eng.* **2016**, *142*, 27–41. [CrossRef]
8. Longo, G.; Gasparella, A. Three years experimental comparative analysis of a desiccant based air conditioning system for a flower greenhouseL Assessment of different desiccants. *Appl. Therm. Eng.* **2015**, *78*, 584–590. [CrossRef]
9. Han, J.; Guo, H.; Brad, R.; Gao, Z.; Waterer, D. Dehumidification requirement for a greenhouse located in a cold region. *Appl. Eng. Agric.* **2015**, *31*, 291–300.

10. Maslak, K.; Nimmermark, S. Thermal energy use for dehumidification of a tomato greenhouse by natural ventilation and a system with an air-to-air heat exchanger. *Agric. Food Sci.* **2017**, *26*, 56–66. [CrossRef]
11. Holladay, M.; Preventing Frost Buildup in HRVs and ERVs. Green Building Advisor. 2018. Available online: https://www.greenbuildingadvisor.com/article/preventing-frost-buildup-in-hrvs-and-ervs (accessed on 15 September 2022).
12. McColl, K. HRVs Work in Cold Climates, Experts Insist, but Need to Be Operated Properly. CBC. 2018. Available online: https://www.cbc.ca/news/canada/north/hrvs-in-northern-climates-1.4572908 (accessed on 15 September 2022).
13. Ahamed, S.; Guo, H.; Taylor, L.; Tanino, K. Heating demand and economic feasibility analysis for year-round vegetable production in Canadian Prairies greenhouses. *Inf. Process. Agric.* **2019**, *6*, 81–90. [CrossRef]
14. Kowalczyk, K.; Olewnicki, D.; Mirgos, M.; Gajc-Wolska, J. Comparison of Selected Costs in Greenhouse Cucumber Production with LED and HPS Supplemental Assimilation Lighting. *Agronomy* **2020**, *10*, 1342. [CrossRef]
15. Slattery, R.A.; VanLoocke, A.; Bernacchi, C.J.; Zhu, X.-G.; Ort, D.R. Photosynthesis, Light Use Efficiency, and Yield of Reduced-Chlorophyll Soybean Mutants in Field Conditions. *Front. Plant Sci.* **2017**, *8*, 549. [CrossRef] [PubMed]
16. Katzin, D.; Marcelis, L.F.; van Mourik, S. Energy savings in greenhouses by transition from high-pressure sodium to LED lighting. *Appl. Energy* **2021**, *281*, 116019. [CrossRef]
17. Katzin, D.; van Mourik, S.; Kempkes, F.; van Henten, E.J. GreenLight—An open source model for greenhouses with supplemental lighting: Evaluation of heat requirements under LED and HPS lamps. *Biosyst. Eng.* **2020**, *194*, 61–81. [CrossRef]
18. Nauta, A.; Lubitz, W.; Tasnim, S.; Han, J. Development and Evaluation of a New Greenhouse Energy Model with Data from Four Ontario Greenhouses. In Proceedings of the Canadian Greenhouse Conference, Niagara Falls, ON, Canada, 6–7 October 2021.
19. Nauta, A.L.; Lubitz, W.D.; Tasnim, S.Y.; Mahmud, S.H. Thermal modelling of greenhouse using 1D lumped capacitance model. In Proceedings of the 5th International Conference of the International Commission of Agricultural and Biosystems Engineering, Quebec City, QC, Canada, 10–14 May 2021.
20. Nauta, A.; Lubitz, W.D.; Tasnim, S.H.; Han, J. Methodology and Validation of a New Climate Prediction Model for Commercial and Small-Scale Greenhouses. In Proceedings of the 2022 Responsible Engineering and Living Symposium, Windsor, ON, Canada, 23–24 June 2022. [CrossRef]
21. Mashonjowa, E.; Ronsse, F.; Milford, J.; Pieters, J. Modelling the thermal performance of a naturally ventilated greenhouse in Zimbabwe using a dynamic greenhouse climate model. *Sol. Energy* **2013**, *91*, 381–393. [CrossRef]
22. Blanchard, M.G.; Runkle, E.; Both, A.-J.; Shimizu, H. Greenhouse Energy Curtains Influence Shoot-tip Temperature of New Guinea Impatiens. *Hortscience* **2012**, *47*, 483–488. [CrossRef]
23. Vanthoor, B.; Stanghellini, C.; van Henten, E.; de Visser, P. A methodology for model-based greenhouse design: Part 1, a greenhouse climate model for a broad range of designs and climates. *Biosyst. Eng.* **2011**, *110*, 363–377. [CrossRef]
24. Ghose, S. Thermal Modelling of Passive Solar High Tunnels Located at the Guelph Centre for Urban Organic Farming. Master's Thesis, University of Guelph, Guelph, ON, Canada, 2018. Available online: https://atrium.lib.uoguelph.ca/xmlui/handle/10214/14173 (accessed on 12 March 2022).
25. Lubitz, W.D. Reducing Canadian Greenhouse Energy Costs Using Highly Insulating Glazing. In *Renewable Energy in the Service of Mankind I*; Springer International Publishing: Cham, Switzerland, 2015; pp. 649–658. [CrossRef]
26. Government of Canada. Engineering Climate Datasets. 2021. Available online: https://climate.weather.gc.ca/prods_servs/engineering_e.html (accessed on 12 March 2022).
27. Koroleva, A. Efficiency of Heat Recovery Units in Ventilation. Bachelor's Thesis, Building Services Engineering, Mikkeli University of Applied Sciences, Mikkeli, Finland, 2012.
28. Stull, R. Moisture. In *Meteorology for Scientists and Engineers*, 3rd ed.; University of British Columbia: Vancouve, BC, Canada, 2015.
29. Huang, J. A Simple Accurate Formula for Calculating Saturation Vapor Pressure of Water and Ice. *J. Appl. Meteorol. Clim.* **2018**, *57*, 1265–1272. [CrossRef]
30. Michael, P.R.; Johnston, D.E.; Moreno, W. A conversion guide: Solar irradiance and lux illuminance. *J. Meas. Eng.* **2020**, *8*, 153–166. [CrossRef]
31. Torres, A.; Lopez, R. Commercial Greenhouse Production: Measuring Daily Light Integral in a Greenhouse. 2008. Available online: https://www.extension.purdue.edu/extmedia/ho/ho-238-w.pdf (accessed on 22 November 2021).
32. DLC. DLC Qualified Product Lists. 2020. Available online: https://qpl.designlights.org/horticulture#page-2 (accessed on 14 January 2022).
33. Moody, E. How LED and HPS Lighting Affects Air and Leaf Temperature. 2019. Available online: https://pllight.com/how-led-and-hps-lighting-can-affect-air-and-leaf-temperature/ (accessed on 3 July 2021).
34. Ontario Energy Board. Historical Natural Gas Rates. 2022. Available online: https://www.oeb.ca/consumer-information-and-protection/natural-gas-rates/historical-natural-gas-rates (accessed on 15 September 2022).
35. Epstein, A.; Lubitz, W.; Dineen, G.; Dyck, J. Grain Drying Utilizing Air Source Heat Pumps for Reduced Cost and Greenhouse Gas Emissions. In Proceedings of the CSBE/SCGAB 2018 Annual Conference, Guelph, ON, Canada, 22–25 July 2018.
36. Han, J.; West, J.; Huber, A. Demonstration of Energy-Saving Dehumidification in Ontario Greenhouses. In Proceedings of the Canadian Greenhouse Conference, Niagara Falls, ON, Canada, 7–8 October 2020.
37. Chen, X.; Riffat, S.; Bai, H.; Zheng, X.; Reay, D. Recent progress in liquid desiccant dehumidification and air-conditioning: A review. *Energy Built Environ.* **2020**, *1*, 106–130. [CrossRef]

38. Kumar, K.; Hao, X.; Khosla, S.; Guo, X.; Bennett, N. Comparison of HPS lighting and hybrid lighting with top HPS and intra-canopy LED lighting for high-wire mini-cucumber production. *Acta Hortic.* **2016**, *1134*, 111–118. [CrossRef]
39. Save on Energy. Installing LED Grow Lights in Your Greenhouse. 2022. Available online: https://saveonenergy.ca/For-Business-and-Industry/Resources/Installing-LED-Grow-lights-in-your-greenhouse (accessed on 20 July 2022).
40. Government of Canada. The Federal Carbon Pollution Pricing Benchmark. 2021. Available online: https://www.canada.ca/en/environment-climate-change/services/climate-change/pricing-pollution-how-it-will-work/carbon-pollution-pricing-federal-benchmark-information.html (accessed on 20 April 2022).